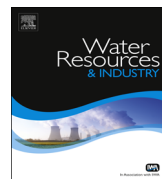




ELSEVIER

Contents lists available at ScienceDirect

## Water Resources and Industry

journal homepage: [www.elsevier.com/locate/wri](http://www.elsevier.com/locate/wri)

CrossMark

# Kinetic, equilibrium and thermodynamic studies of synthetic dye removal using pomegranate peel activated carbon prepared by microwave-induced KOH activation

Mohd Azmier Ahmad<sup>a</sup>, Nur Azreen Ahmad Puad<sup>a</sup>,  
Olugbenga Solomon Bello<sup>a,b,\*</sup>

<sup>a</sup> School of Chemical Engineering, Engineering Campus, Universiti Sains Malaysia, 14300 Nibong Tebal, Penang, Malaysia

<sup>b</sup> Department of Pure and Applied Chemistry, Ladoko Akintola University of Technology, P.M.B 4000, Ogbomoso, Oyo State, Nigeria

## ARTICLE INFO

### Article history:

Received 17 March 2014

Received in revised form

10 June 2014

Accepted 26 June 2014

### Keywords:

Pomegranate peel

Remazol brilliant blue reactive dye

Adsorption

Spontaneous

## ABSTRACT

Pomegranate peel was converted into activated carbon using microwave induced and KOH activation techniques. The prepared activated carbon (PPAC) was characterized using FTIR, TGA, SEM, and nitrogen-adsorption surface area (BET). BET measurements gave remarkable increase in both the surface area (941.02 m<sup>2</sup>/g) and total pore volume (0.470 cm<sup>3</sup>/g). Various operational parameters such as pH, initial dye concentration, contact time and solution temperature in batch systems were investigated on the use of PPAC in the adsorption of remazol brilliant blue reactive (RBBR) dye. At pH 2, the optimum dye removal was 94.36%. The amount of dye removed was dependent on initial dye concentration and solution temperature. Adsorption kinetics was found to follow pseudo-second-order kinetic model. Experimental data were analyzed using eight model equations: Langmuir, Freundlich, Temkin, Dubinin–Radushkevich, Radke Prausnitz, Sips, Viet–Sladek and Brouers – Sotolongo isotherms and it was found that the Freundlich isotherm model fitted the adsorption data most with the highest correlation ( $R^2 \geq 0.99$ ) and lowest normalized standard deviation,  $\Delta q_e$ . Both intra-particle and film diffusion governed the adsorption process. Thermodynamic parameters,

\* Corresponding author at: Department of Pure and Applied Chemistry, Ladoko Akintola University of Technology, P.M.B 4000, Ogbomoso, Oyo State, Nigeria.

E-mail address: [osbello06@gmail.com](mailto:osbello06@gmail.com) (O.S. Bello).

<http://dx.doi.org/10.1016/j.wri.2014.06.002>

2212-3717/© 2014 The Authors. Published by Elsevier B.V. This is an open access article under the CC BY-NC-ND license (<http://creativecommons.org/licenses/by-nc-nd/3.0/>).

such as standard Gibbs free energy ( $\Delta G^0$ ), standard enthalpy ( $\Delta H^0$ ), standard entropy ( $\Delta S^0$ ), and the activation energy ( $E_a$ ) were calculated. The adsorption of RBBR dye onto PPAC was found to be spontaneous and exothermic in nature. This study shows that the adsorption follows physisorption mechanism.

© 2014 The Authors. Published by Elsevier B.V. This is an open access article under the CC BY-NC-ND license (<http://creativecommons.org/licenses/by-nc-nd/3.0/>).

## 1. Introduction

The disposal of textile waste water is currently a major problem from a global viewpoint. Textile industries produce a lot of wastewater, which contains several contaminants, including acidic or caustic dissolved solids, toxic compounds, and dyes [1]. Among textile effluents, synthetic dyes are hardly eliminated under aerobic conditions and are probably decomposed into carcinogenic aromatic amines under anaerobic conditions [2]. Also, it is difficult to remove reactive dyes using chemical coagulation due to the dyes' high solubility in water [3]. Synthetic dyes are commonly used in many industries such as textile, leather, tanning, paper, rubber, plastics, cosmetics, pharmaceutical and food industries. Synthetic dyes, classified by their chromophores, have different stable chemical structures and are not often degraded or removed by conventional physical and chemical processes [3,4]. These dyes contain chromophoric groups such as azo, anthraquinone, triarylmethane etc. and reactive groups e.g. vinyl sulfone, chlorotriazine, trichloropyrimidine etc. Remazol Brilliant Blue R (RBBR) is one of the most important dyes in the textile industry. RBBR, ananthraquinone derivative, represents an important class of toxic and recalcitrant organo pollutants [5–7]. Adsorption with activated carbon appears to be the best prospect of eliminating this dye. In spite of its good efficiency, this adsorbent is expensive and difficult to regenerate after use. Therefore, many researches in recent years have focused on the use of various low-cost adsorbents instead of activated carbon: banana stalk [8], groundnut hull [9], oil palm fruit fiber [10], cocoa pod husks [11], mango peels [12], rice husks [13–16], periwinkle shell [17], coconut shell [18], *Imperata cylindrica* leaf [19], rubber seed coat [20], fly ash [21], activated carbon [22], coconut shell [23], Jerusalem artichoke [24], maize stem tissue [25], electro coagulation using solar energy [26] and electro coagulation process [27].

In this study, pomegranate peel activated carbon (PPAC) was evaluated as a new adsorbent for removal of a synthetic dye from aqueous solution. We examined the effects of solution pH, contact time, initial dye concentration and temperature on RBBR dye adsorption process onto PPAC from aqueous solution. FTIR analysis was carried out to understand the surface functional groups on the adsorbent. Equilibrium data were analyzed by eight different equilibrium isotherm models. Kinetic data were evaluated by pseudo-first order, pseudo-second order, Elovich and Avrami models. Thermodynamic parameters such as free energy ( $\Delta G$ ), enthalpy ( $\Delta H$ ) and entropy ( $\Delta S$ ) were also determined to understand the spontaneity of the adsorption process

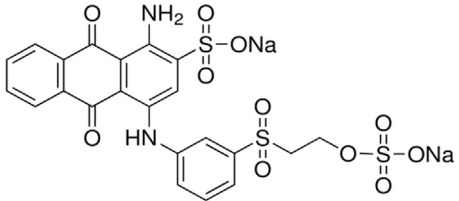
## 2. Materials and methods.

### 2.1. Preparation of activated carbon

Pomegranate peel (PP), was washed thoroughly with distilled water to remove adhering dirt particles from the surface. PP was dried in an oven at 70 °C, cut, grounded with a grinder and screened to a particle size of 1–2 mm. The carbonization process was carried out by loading 200 g of dried precursor into a tubular furnace, and heating to a carbonization temperature of 700 °C for 30 min under purified N<sub>2</sub> flow [28]. The char produced was mixed with KOH pellets at different impregnation Ratio (IR), defined as:

$$IR = \frac{W_{KOH}}{W_{char}} \quad (1)$$

**Table 1**  
Properties of Remazol brilliant blue Reactive dye.

Properties	
Chemical name	Disodium 1-amino-9, 10-dioxo-4-[3-(2-sulfonatooxyethylsulfonyl) anilino]anthracene-2-sulfonate
Common name	Remazol brilliant blue R
Generic name	Reactive blue 19
CAS number	2580-78-1
Color index number	61,200
Ionization	Reactive
Maximum wavelength	590 nm
Empirical formula	C <sub>22</sub> H <sub>16</sub> N <sub>2</sub> Na <sub>2</sub> O <sub>11</sub> S <sub>3</sub>
Molecular weight	626.54 g/mol
Chemical structure	

where  $w_{KOH}$  and  $w_{char}$  is the dry weight of KOH pellets (g) and char (g) respectively. A modified microwave oven with a frequency of 2.45 GHz was employed for the activation step. Nitrogen gas at a pre-set flow rate (300 cm<sup>3</sup>/min) was used to purge air from the reactor before the start of microwave heating and it continued to flow during the activation stage. The oven has a power controller to select different power levels and a timer for various exposure times at a set microwave power level. The resultant activated carbon (PPAC) was washed sequentially with 0.1 M hydrochloric acid. It was then washed with water until the pH of the washing solution reached 6.5–7. The yield is defined as the dry weight of activated carbon per weight of char utilized for activation.

$$\text{Yield(\%)} = \frac{W_c}{W_0} \times 100 \quad (2)$$

### 2.1.1. Adsorbate used

Remazol brilliant blue R (RBBB) dye was used as adsorbate to determine the adsorption performance of the prepared activated carbon. The properties of RBBB dye used are listed in Table 1.

### 2.1.2. Batch equilibrium studies

The effects of initial dye concentration, contact time, solution temperature and solution pH on the adsorption uptake for adsorption of RBBB dye onto PPAC were studied. Sample solutions were withdrawn at intervals to determine the residual concentration by using UV–vis spectrophotometer at the maximum wavelength of 590 nm. The amount of dye adsorbed at equilibrium,  $q_e$  (mg/g) was calculated as:

$$q_e = \frac{(C_o - C_e)V}{W} \quad (3)$$

where  $C_o$  and  $C_e$  (mg/L) are the liquid-phase concentrations of initial adsorbate and equilibrium, respectively.  $V$  is the volume of the solution (dm<sup>3</sup>) and  $W$  is the mass (g) of PPAC used.

### 2.1.3. Effect of initial adsorbate concentration and contact time

100 ml of RBBB dye solution with known initial concentration was put in a series of 250 ml Erlenmeyer flasks. The amount of adsorbent that was added into each flask was fixed at 0.1 g. The flasks were placed in an isothermal water bath shaker (Model Protech, Malaysia) at constant temperature of 30 °C, with rotation speed of 120 rpm, until equilibrium point was reached. Samples

are withdrawn at intervals to determine the residual concentration of the dye at 590 nm wavelength using a UV–vis Spectrophotometer.

#### 2.1.4. Effect of solution pH

Solution pH was studied by varying the initial pH of solution from 2 to 12. The pH was adjusted by 0.1 M NaOH or 0.1 M HCl and measured by using a pH meter. The adsorbent dosage, rotation speed, solution temperature and initial dye concentration were fixed at 0.1g, 120 rpm, 30 °C and 100 mg/L respectively.

#### 2.1.5. Adsorption isotherm studies

This was carried out by fitting the equilibrium data to the Langmuir [29], Freundlich [30], Temkin [31], Dubinin–Radushkevich [32], Sips [33], Vieth–Sladek [34], Bruoers–Sotolongo [35] and Radke–Prausnitz isotherms [36]. The applicability and suitability of the isotherm equation to the equilibrium data were compared by judging the values of the correlation coefficients,  $R^2$  and normalized standard deviation,  $\Delta q_e$ . Linear regression was carried out by using Microsoft Excel spreadsheet with Solver add-in to determine the isotherm parameters.

### 2.2. Batch kinetic studies

This procedure is similar to that of batch equilibrium studies. The difference is that the absorbent–absorbate solution was taken at preset time intervals and the concentration of the solution was measured. The amount of adsorption at time  $t$ ,  $q_t$  (mg/g), was calculated using Eq. (4)

$$q_t = \frac{(C_o - C_t)V}{W} \quad (4)$$

where  $C_o$  and  $C_t$  (mg/L) are the liquid-phase concentrations of adsorbate at initial and at any time  $t$ , respectively.  $V$  is the volume of the solution and  $W$  is the mass of adsorbent used. The adsorption kinetics of dye on adsorbent was investigated using pseudo-first order model, pseudo-second-order model, Avrami, and Elovich models respectively.

#### 2.2.1. Pseudo-first-order kinetic model

The pseudo-first-order kinetic model equation is generally expressed as follows [37]:

$$\ln(q_e - q_t) = \ln q_e - k_1 t \quad (5)$$

where  $q_e$  is the amount of adsorbate adsorbed at equilibrium, (mg/g),  $q_t$  is the amount of solute adsorb per unit weight of adsorbent at time, (mg/g),  $k_1$  is the rate constant of pseudo-first order sorption ( $1/h$ ). A plot of  $\ln(q_e - q_t)$  versus  $t$  gives a straight line with slope of  $k_1$  and intercept of  $\ln q_e$ .

#### 2.2.2. Pseudo-second-order kinetic model

The pseudo-second-order equation can be expressed as [38]:

$$\frac{t}{q_t} = \frac{1}{k_2 q_e^2} + \frac{1}{q_e} t \quad (6)$$

The linear plot of  $t/q_e$  versus  $t$  gives  $1/q_e$  is the slope and  $1/h$  is the intercept.

#### 2.2.3. Elovich kinetic model

The simplified Elovich equation expressed as [39]:

$$q_t = \frac{1}{\beta} \ln(\alpha\beta) + \frac{1}{\beta} \ln t \quad (7)$$

where  $\alpha$  is the initial desorption rate (mg/(g min)) and  $\beta$  is the desorption constant (g/mg) during any experiments. Plot of  $q_t$  versus  $\ln t$  gave a linear relationship with slope of  $1/\beta$  and an intercept of  $(1/\beta) \ln(\alpha\beta)$ . The  $1/\beta$  value reflects the number of sites available for adsorption whereas the value of  $(1/\beta) \ln(\alpha\beta)$  indicates the adsorption quantity when  $\ln t$  equal to zero.

#### 2.2.4. Avrami kinetic model

The Avrami equation is used to verify specific changes of kinetic parameters as functions of the temperature and reaction time. It is also an adaptation of kinetic thermal decomposition modeling [40].

The Avrami kinetic model is expressed as:

$$q_t = q_e \{ 1 - \exp[-(K_{AV}t)^{n_{AV}}] \} \quad (8)$$

where  $q_t$  is the adsorption fraction at time  $t$ ,  $k_{AV}$  is the adjusted kinetic constant, and  $n_{AV}$  is another constant, which is related to the adsorption mechanism.  $n$  value can be used to verify possible interactions of the adsorption mechanisms in relation to the contact time and the temperature.

#### 2.2.5. Validity of kinetic model

The applicability and fitting of the isotherm equation to the kinetic data was compared by judging from the  $R^2$  values and the normalized standard deviation  $\Delta q_t$  (%) calculated from Eq. (9). The normalized standard deviation,  $\Delta q_t$  (%) was used to verify the kinetic model used to describe the adsorption process. It defines as:

$$\Delta q = 100 \frac{\sqrt{\sum \left( \frac{q_{e,exp} - q_{e,cal.}}{q_{e,exp}} \right)^2}}{n - 1} \quad (9)$$

where  $n$  is the number of data points,  $q_{exp}$  and  $q_{cal}$  (mg/g) are the experimental and calculated adsorption capacity values. Lower value of  $\Delta q_t$  indicates good fit between experimental and calculated data.

### 2.3. Adsorption thermodynamics

The experimental data obtained from batch adsorption studies performed earlier were analyzed by using the thermodynamic equations as expressed by Eq. (10).

$$\Delta G = -RT \ln K_L \quad (10)$$

$$\ln K = \frac{\Delta S}{R} - \frac{\Delta H}{RT} \quad (11)$$

$\Delta G$  was calculated using Eq. (10). The values of  $\Delta H$  and  $\Delta S$  can be obtained respectively from the slope and intercept of Van't Hoff plot of  $\ln K_L$  versus  $1/T$ . Values of  $K_L$  may be calculated from the relation  $\ln q_e/C_e$  at different solution temperatures of 30, 45 and 60 °C respectively. Arrhenius equation has been applied to evaluate the activation energy of adsorption representing the minimum energy that reactants must have for the reaction to proceed, as shown by following relationship:

$$\ln k_2 = \ln A - \frac{E_a}{RT} \quad (12)$$

where  $k_2$  is the rate constant obtained from the pseudo-second-order kinetic model, (g/mg h),  $E_a$  is the Arrhenius activation energy of adsorption, (kJ/mol),  $A$  is the Arrhenius factor,  $R$  is the universal gas constant (8.314 J/mol K) and  $T$  is the absolute temperature. When  $\ln k_2$  is plotted against  $1/T$ , a straight line with slope of  $-E_a/R$  is obtained.

### 2.4. Adsorption mechanism

The adsorption mechanisms of RBBB dye on the adsorbent were investigated using intraparticle diffusion model [41] represented by Eq. (13). The applicability and fitting of the model throws more light into the mechanism of RBBB dye adsorption onto PPAC prepared.

$$q_t = k_{pi}t^{1/2} + C_i \quad (13)$$

where  $C_i$  is the intercept and  $k_{pi}$  (mg/g h<sup>1/2</sup>) is the intraparticle diffusion rate constant, which can be evaluated from the slope of the linear plot of  $q_t$  versus  $t^{1/2}$ . The  $q_t$  is the amount of solute adsorb per unit weight of adsorbent per time, (mg/g), and  $t^{1/2}$  is the half adsorption time, (g/h mg). The intercept

**Table 2**  
Surface area and pore characteristics of the samples.

Sample	BET surface area (m <sup>2</sup> /g)	Mesopore surface area (m <sup>2</sup> /g)	Total pore volume (cm <sup>3</sup> /g)	Average pore diameter (nm)
PP	5.04	–	–	–
PP char	115.30	74.83	0.120	2.86
PPAC	941.02	556.17	0.470	2.76

**Table 3**  
Proximate and elemental analysis of prepared samples.

Sample	Proximate analysis (%)				Elemental analysis (%)			
	Moisture	Volatile	Fixed Carbon	Ash	C	H	S	(N+O) <sup>a</sup>
PP	7.90	65.10	22.02	4.98	28.46	5.70	0.08	65.76
PP char	3.15	20.65	72.36	3.84	71.80	2.79	0.04	25.37
PPAC	2.04	14.37	79.80	3.79	78.34	1.35	0.01	20.30

<sup>a</sup> Estimated by difference.

of the plot reflects the boundary layer effect. The larger the intercept, the greater the contribution of the surface sorption in the rate-controlling step. If the regression of  $q_t$  versus  $t^{1/2}$  is linear, and passes through the origin, then intraparticle diffusion is the sole rate-limiting step. If the linear plots at each concentration did not pass through the origin, it indicates that the intraparticle diffusion was not only rate controlling step [42].

### 3. Results and discussions

#### 3.1. Characterization of PPAC

The pomegranate peel (PP), PP char and PPAC samples prepared were characterized using the BET surface area, proximate analysis, elemental analysis, surface morphology and FTIR techniques.

##### 3.1.1. BET surface area and pore characteristics

Table 2 shows the BET surface area and pore characteristics of PP, PP char and PPAC samples. The BET surface area and total pore volume for PPAC were 941.02 m<sup>2</sup>/g and 0.47 cm<sup>3</sup>/g, respectively, these values are comparable with the commercial F300 and F400 AC from Merck [43] which were reported to have BET surface area of 957 and 960 m<sup>2</sup>/g and total pore volume of 0.525 and 0.56 cm<sup>3</sup>/g, respectively. The average pore diameter for PPAC was 2.76 nm. It belongs to the mesopore region according to IUPAC classification [44]. The microwave assisted KOH activation step had contributed to the high surface area and total pore volume of the PPAC which were advantageous for dye adsorption. The intercalation of the KOH with carbon was important in the generation of well-developed pores thus creating large surface area and high pore volume [45].

##### 3.1.2. Proximate and elemental analysis

Proximate and elemental analysis of the PP, PP char and PPAC samples are shown in Table 3. PP was found to have the highest moisture and volatile matter but with lowest fixed carbon and ash contents. The results showed that the moisture and volatile content decreased significantly during the microwave assisted activation process. During this process, organic substances in the sample become

**Table 4**  
FTIR spectra band assignments for PP, PP char and PPAC.

Assignment	Band position (cm <sup>-1</sup> )		
	PP	PP char	PPAC
O–H stretching of hydroxyl group	3730–3298	–	–
C≡C stretching of alkyne group	2916–2341	2384–2067	2360–2087
C=O stretching of lactones, ketones, and carboxylic anhydrides	1901–1736	1940–1994	1940–1998
C–O stretching vibrations in quinine structure	1647	–	–
C=C of aromatic ring	1462	1585	1585
C–H stretching in alkanes or alkyl group	1361	1354	–
C–O groups stretching in ester, ether or phenol group	1246–1169	–	–
C–N stretching of aliphatic primary amine	1049	–	–
–C≡C–H bend in functional group	895–667	698	–

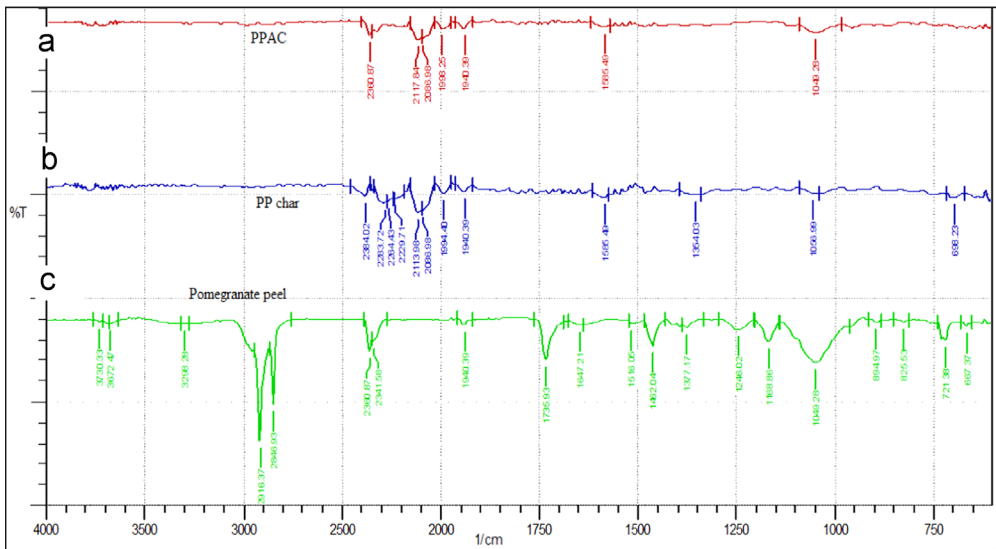


**Fig. 1.** FTIR spectra; (a) PP; (b) PP char; and (c) PPAC.

unstable and the bonding or linkage of the molecules breaks. The activation process also caused the volatile matter to be discharged as gas and liquid products leaving the material with high carbon content [46]. The result from elemental analysis showed that the carbon content increased significantly from 28.46% to 78.34% while the other element such as hydrogen (H), sulfur (S), nitrogen (N) and oxygen (O) decreased after the microwave assisted activation step. This was attributed to the decomposition of volatile compounds and degradation of organic substances under microwave irradiation leaving a high purity carbon [47].

### 3.1.3. Fourier transform infra red spectra

Table 4 shows the tabulated data for FTIR spectra band assignments for PP, PP char, and PPAC samples obtained from Fig. 1. These spectral describe the various changes that occurred in the PP, PP char and PPAC samples. The spectrum for PP shows long bandwidth at 2341–2916 cm<sup>-1</sup> which indicates the C≡C stretching of alkyne group. The C–N stretching of aliphatic primary amine group was detected at bandwidths of 1049 cm<sup>-1</sup>. The C=O stretching of lactones, ketones and carboxylic

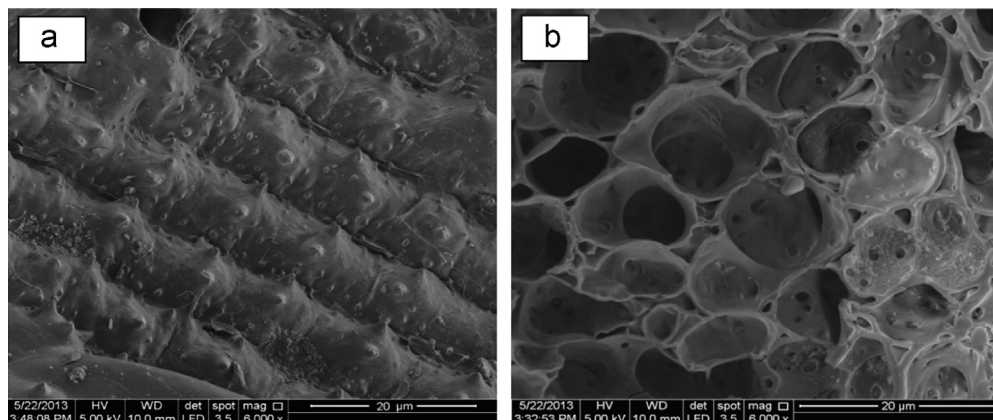


Fig. 2. SEM micrographs of (a) PP (6000 ×); (b) PPAC (6000 ×).

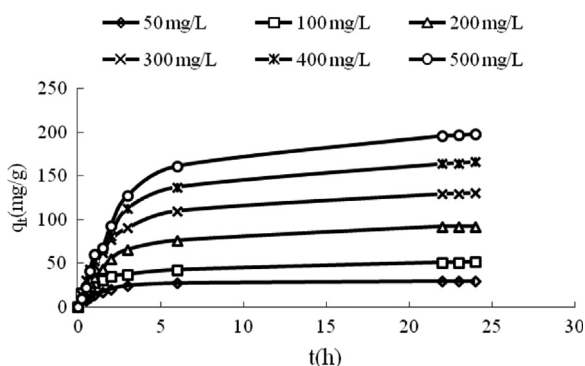


Fig. 3. Plot of adsorption uptake against adsorption time at various initial concentrations at 30 °C.

anhydrides functional groups were detected at bandwidths of 1901–1998  $\text{cm}^{-1}$ . Some of the peaks disappear in PPAC due to heating at high temperature. Similar results was obtained in the study of the effects of acid leaching on porosity and surface functional groups of cocoa (*Theobroma cacao*)-shell based activated carbon [48].

### 3.1.4. Surface morphology

Fig. 2 (a) and (b) showed the surface morphology of PP and the PPAC, respectively at same magnification power (6000 ×). From the SEM micrographs, there was no pore development on the precursor and the surface texture is rough and uneven. However, the surface morphology of the precursor changed after the physicochemical activation step where there are well-developed pores existing on the surface of the PPAC. The surface becomes more rough and uneven. It can be seen that there was a significant difference between the PP and PPAC surface morphology. Pore development was caused by the breakdown of some material in the precursor due to thermal expansion during the activation step [49]. The reaction rate between the activating agent which is KOH and carbon also increase when the precursor is subjected to high activation temperature, thus leading to the formation of well-developed pores [50]. The porosity and surface area of the PPAC increased as the reaction between carbon and KOH led to the formation of new pores due to loss of volatile compound during the physicochemical activation step [51].



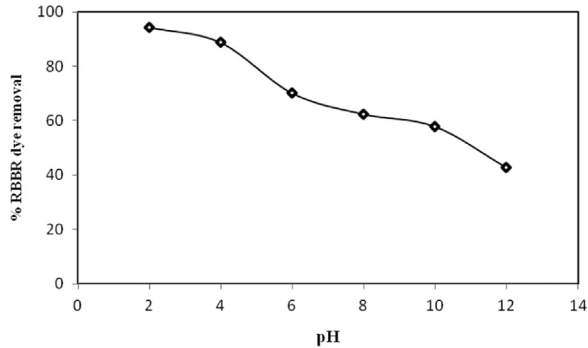


Fig. 4. Effect of initial pH on RBBR dye removal.

### 3.2. Batch adsorption studies

#### 3.2.1. Batch equilibrium studies

3.2.1.1. *Effect of contact time, initial dye concentration on adsorption and solution temperature.* The effect of contact time and initial dye concentration on PPAC is illustrated in Fig. 3. Fig. 3 depicts the dye adsorption uptake versus the adsorption time at various initial dye concentrations ranging from 50–500 mg/L at 30 °C. Similar plots were obtained at 45 °C and 60 °C respectively (Figures not shown). From the Fig. 3, the adsorption uptake of RBBR dye at equilibrium increased from 29.52 to 198.81 mg/L as the initial dye concentration increased from 50 to 500 mg/L. The mass transfer driving force also increased as the initial dye concentration increased. Higher initial dye concentration provides stronger driving force of the concentration gradient resulting in higher adsorption capacity [52]. At lower initial dye concentration, there are considerable amount of active sites on the surface of activated carbon which are available for dye adsorption. The profiles of the adsorption curve were even and continuous approaching equilibrium state gradually. It took 6–22 h for the adsorption process to attain equilibrium at concentrations 50–200 mg/L and 300–500 mg/L respectively. The initial stage of the adsorption gave significant increase in dye adsorption capacity which suggests that a considerable amount of active site on adsorbent's surface was occupied by small amount of adsorbate. At the end of the process, the adsorption capacities become slower due to the saturation of active sites [53].

The effect of different solution temperature on adsorption of RBBR dye onto PPAC was also investigated (Figure not shown). The maximum adsorptions of RBBR dye onto PPAC are 198.81, 237.45 and 278.96 mg/g at 30 °C, 45 °C and 60 °C respectively. The increase is due to increase in dye mobility that may occur at high temperature between the adsorbent and the adsorbate [54]. Adsorption of RBBR dye onto PPAC is an endothermic process; the adsorption capacity increased with increase in solution temperature [55].

#### 3.2.2. Effect of initial solution pH

The pH point of zero charge was found to occur at pH 3.6 meaning that PPAC surface has a positive charge in solution up to pH 3.6 and a negative charge above this pH [56] (Figure not shown). The contents of oxygen-containing functional groups with various acidic groups determined using Boehm titration [57] are: (carboxyl (0.1636 meq g<sup>-1</sup>), lactonic (0.3145 meq g<sup>-1</sup>) and phenolic (0.3026 meq g<sup>-1</sup>), total acidic group (0.7807 meq g<sup>-1</sup>), total amount of the basic groups (0.2533 meq g<sup>-1</sup>). The acidic group content is much higher than the basic groups content. This is consistent with a value of pH<sub>pzc</sub> 3.6, showing the dominance of acidic groups. The effect of initial pH on RBBR dye adsorption onto PPAC is as shown in Fig. 4. The maximum RBBR dye removal of 94.36% was observed at pH 2. The dye adsorption decreased with increase in solution pH. At low pH there is an increase in the H<sup>+</sup> ions in solution. The dye molecule is negatively charged; this result in electrostatic interaction between the dye molecule and the adsorbent resulting in higher percentage dye removal. RBBR dye carries negative charge on their sulfonic (–SO<sub>3</sub>–) functional group; they are attracted to the positively charged adsorbent site at lower pH. On the other hand, a reduction in percentage removal with

increase in solution pH was due to the presence of the negative charge on the adsorbent site thus resulting in electrostatic repulsion between adsorbent and the negatively charged dye molecules. Similar observations were observed in the use of *Jatropha curcas* pods and cocoa pod husk based activated carbon in the adsorption of RBBR dye [45,58].

### 3.3. Adsorption isotherm

Eight different isotherm model equations: Langmuir, Freundlich, Temkin, Dubinin–Radushkevich, Sips, Vieth–Sladek, Brouers–Sotolongo and Radke Prausnitz were chosen to predict the adsorption capacities and fit the experimental equilibrium data. Fig. 5 below showed the plots of the linearized equation isotherm parameters for RBBR dye removal at 30 °C. Table 5 showed the values of maximum adsorption capacities ( $Q_m$ ), correlation coefficients ( $R^2$ ), normalized standard deviations ( $\Delta q_e$ ) and other constant parameters for eight isotherm models equations for the adsorption process at 30 °C. For the Langmuir isotherm, the  $Q_m$  value of 370.86 mg/g was obtained and the value of  $R^2$  of 0.9175 shows good fitting of this isotherm to the experimental data (Table 5). The separation factor ( $R_L$ ), an important parameter of the Langmuir isotherm was 0.3636 (average of six concentrations) indicate favorable adsorption of PPAC-RBBR system. The decrease in  $R_L$  with an increase in the initial concentration indicates that the adsorption is more favorable at high concentrations (Figure not shown). For the Freundlich isotherm, the values of  $n_F=1.49$  and  $1/n_F=0.6695$  indicate that both the physical process and the normal Langmuir isotherm are favorable. The fitting of the Freundlich isotherm to the experimental data is ( $R^2=0.999$ ). For the Temkin isotherm, the constant  $B$  is related to the heat of adsorption, and the positive value found ( $B=62.008$ ) indicates an endothermic process. The fit to experimental data ( $R^2=0.928$ ).

The Sips isotherm is a combination of the Langmuir and Freundlich isotherms. The value of  $Q_m=375.18$  mg/g found for the Sips isotherm is almost the same as value of  $Q_m$  for Langmuir isotherm. Similarly, the Vieth–Sladek isotherm showed a  $Q_m$  equal to 364.59 mg/g. The fit of the Sips isotherm ( $R^2=0.996$ ), the Vieth–Sladek isotherm ( $R^2=0.978$ ). The Brouers–Sotolongo isotherm shows a  $Q_m$  value (327.85 mg/g) lower than that of Langmuir isotherm value. On the other hand, the  $Q_m$  value equal to 386.72 mg/g found for the Radke–Prausnitz isotherm was the highest in all. The fits of the Radke–Prausnitz ( $R^2=0.994$ ), Brouers–Sotolongo ( $R^2=0.968$ ), and the D–R ( $R^2=0.725$ ) isotherms to the experimental data are shown in Table 5. From the analysis of all the isotherms and the knowledge of the most important parameters ( $Q_m$  and  $R^2$ ), the isotherms can be arranged according to their capacity to predict or their efficiency in predicting the experimental behavior of the PPAC-RBBR system. With respect to  $Q_m$  (in descending order): Radke–Prausnitz > Sips > Langmuir > Vieth–Sladek > Brouers–Sotolongo. With respect to  $R^2$  (in descending order): Freundlich > Sips > Radke–Prausnitz > Vieth–Sladek > Brouers–Sotolongo > Temkin > Langmuir > Dubinin–Radushkevich. The normalized standard deviations ( $\Delta q$ ) measures the differences in the amount of dye taken up by the adsorbent predicted by the models and the measured experimentally. According to Table 5, the ( $\Delta q$ ) values of isotherm models ranged from 2.1736 to 105.1379. The Freundlich model presented the lowest  $\Delta q$ , and the highest  $R^2$  value. Therefore, considering the highest  $R^2$  values and the lowest  $\Delta q$  value, the Freundlich model is the most appropriate for the adsorption of the RBBR dye onto PPAC. The value of  $E$  obtained in D–R isotherm was found to be 6.738 kJ mol<sup>-1</sup> (Table 5). Since  $E < 8$  kJ mol<sup>-1</sup>, it suggests that the adsorption mechanism is physical in nature [59]. Comparison of maximum monolayer adsorption capacities of RBBR dye onto various adsorbents were reported in Table 6. PPAC was found to be more effective than other adsorbents reported in literature [60–65].

#### 3.3.1. Variation of $R_L$ with temperature

Fig. 6 below shows the plots of separation factor,  $R_L$  against the initial dye concentration,  $C_0$  at different solution temperatures. The  $R_L$  values indicate the fundamental feature of Langmuir isotherm indicating whether the adsorption process is favorable or unfavorable. The value of  $R_L < 1$  and  $R_L > 1$  indicates the favorable and unfavorable adsorption, respectively. The  $R_L$  values obtained for RBBR dye at three different temperatures are less than 1, which indicates that the adsorption was favorable at

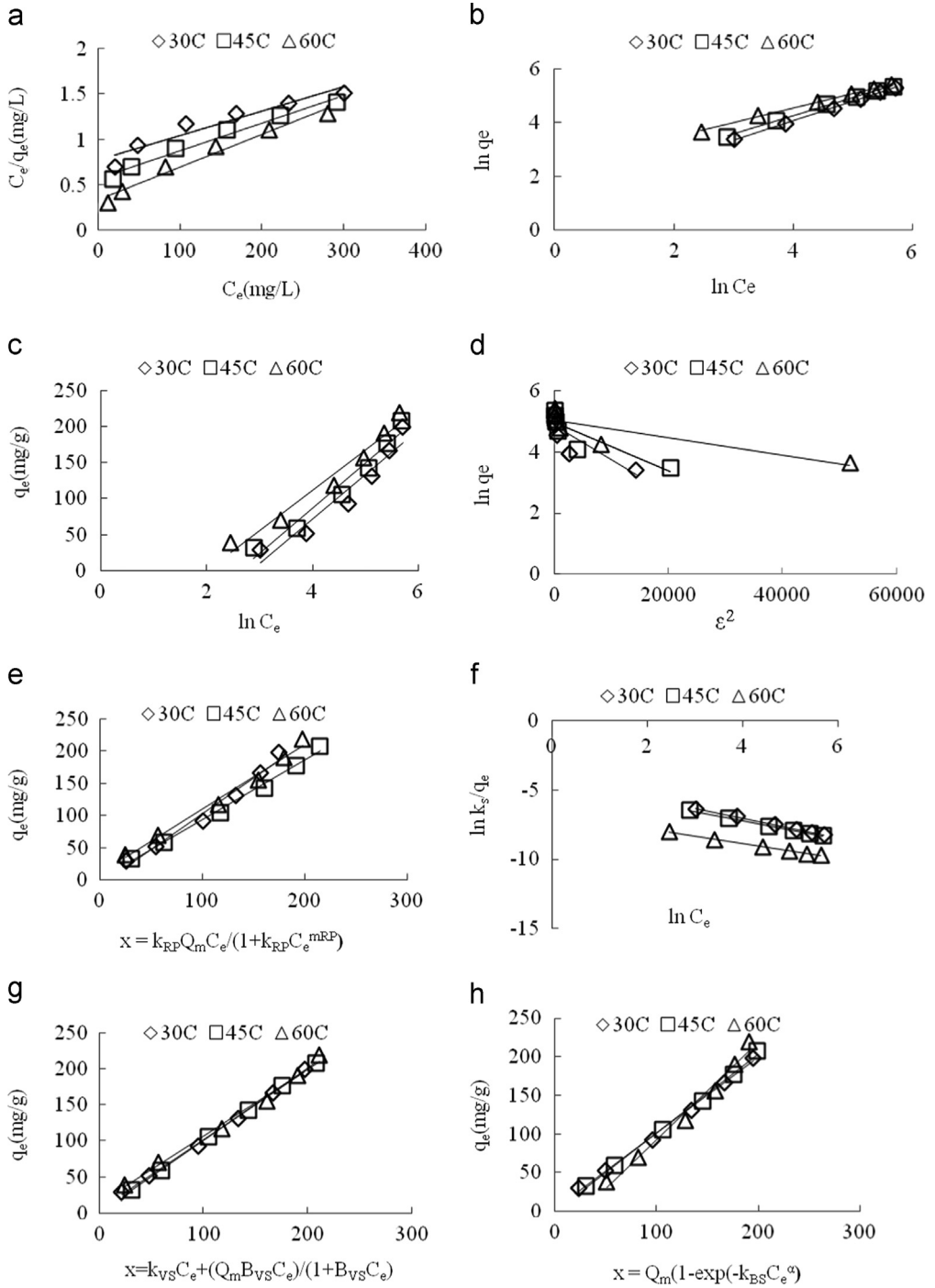


**Fig. 5.** Plots of (a) Langmuir, (b) Freundlich, (c) Temkin, (d) Dubinin–Radushkevich, (e) RadkePrausnite, (f) Sips, (g) Vieth-Sladek, (h) Brouers–Sotolongo isotherms for RBBR dye adsorption on PPAC at 30 °C.

**Table 5**  
Isotherm parameters for RBBR dye adsorption unto PPAC at 30 °C.

PPAC-RBBR															
Langmuir	Freundlich		Temkin		Dubinin-Radushkevich		Sips	Vieth-Sladek		Bruouers-Sotolongo		Radke-Prausnitz			
$Q_m$	370.86	$1/n_F$	0.6695	$B$	62.00806	$b_{DR}$	0.000110137	$Q_m$	375.1800	$K_{vs}$	0.1019	$Q_m$	327.85	$K_{RP}$	0.0035
$K_L$	0.0035	$K_F$	3.3039	$A$	0.058255	$E$	6.73779	$K_s$	0.0514	$Q_m$	364.59	$k_{BS}$	0.0045	$Q_m$	386.72
$R^2$	0.9175	$R^2$	0.9991	$R^2$	0.928295	$q_s$	4.8544	$m_s$	0.7083	$\beta_{vs}$	0.0028	$\alpha$	0.9301	$m_{RP}$	1.0421
$R_L$	0.3636	$n_F$	1.4937		$R^2$	0.7249		$R^2$	0.9955	$R^2$	0.9782	$R^2$	0.968375	$R^2$	0.9936
$\Delta q_e$	9.1150	$\Delta q_e$	2.1736	$\Delta q_e$	4.784	$\Delta q_e$	105.1349	$\Delta q_e$	91.5874	$\Delta q_e$	12.2848	$\Delta q_e$	9.680627	$\Delta q_e$	9.5972

**Table 6**  
Comparison of maximum monolayer adsorption capacities of RBBR dye unto various adsorbents.

Adsorbents	$Q_m$ (mg/g)	References
Polyaniline/chitosan	303.03	61
Polyaniline doped p-Toluene sulfonic acid	28.27	62
Polyaniline camphor sulfonic acid	42.00	62
Polyaniline/EPS	361.82	63
Fly ash	135.70	64
Scenedesmus quadricauda	45.70	65
Periwinkle shell activated carbon	312.64	60
PPAC	370.86	This study

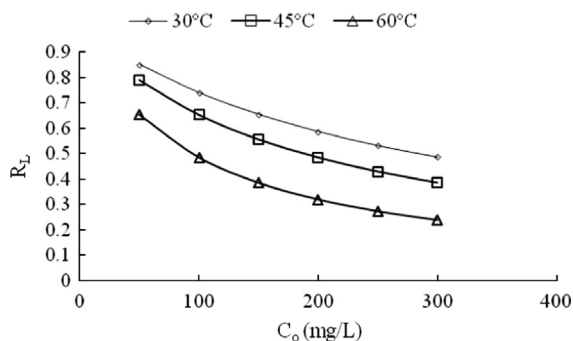


**Fig. 6.** Plots of separation factor against initial dye concentration at different temperatures.

the concentration range studied.  $R_L$  values decreased with increase in initial dye concentration. This shows that the adsorption process is favorable at higher dye concentration [66].

### 3.4. Batch kinetic studies

Adsorption kinetic studies are important in optimizing the process condition for dye adsorption onto adsorbents. The adsorption kinetics of RBBR dye was analyzed using four different models; pseudo-first order, pseudo-second order, Avrami and Elovich models. Fig. 7 below showed the Linearized plots of four models for RBBR dye adsorption unto PPAC at 30 °C. Table 7 reports the kinetic model parameters and their constant values as calculated from various plots at 30 °C. The summary of kinetic model constant values for RBBR dye adsorption given in Table 6 showed that the pseudo-second-order kinetic models fit well with the experimental data compared to the other kinetic

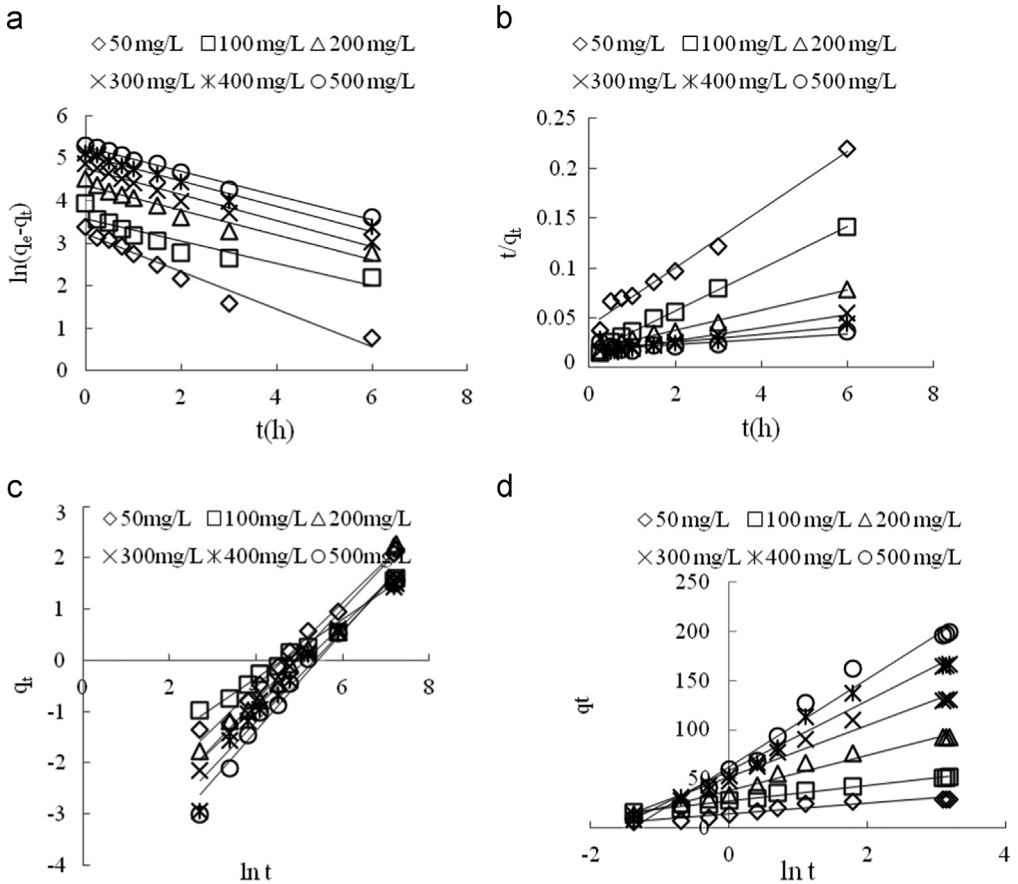


Fig. 7. Linearized plots of (a) Pseudo-first-order, (b) Pseudo-second-order, (c) Avrami, and (d) Elovich kinetic model for RBBR dye adsorption onto PPAC at 30 °C

models. The average  $R^2$  and  $\Delta q_t$  value for pseudo-second-order kinetic models is 0.9842 and 16.285%, respectively. Thus, the adsorption of RBBR dye onto PPAC followed pseudo-second-order kinetic model. The rate coefficient,  $k_2$  of pseudo-second-order for RBBR dye was found to decrease with increase in initial dye concentration. This is due to greater competition for the adsorbent site at higher dye initial concentration. Besides, the electrostatic interaction also decreased on the adsorbent site as the initial concentration increased, thus the dye affinity towards adsorbent reduced. The result is in agreement with the other studied on MG removal by cocoa shell activated carbon [67,68]. For Elovich model, the constant  $\alpha_{EI}$  was decreasing with the increase in initial dye concentration. However, the constant  $\beta_{EI}$  increased as the initial dye concentration increased. This behavior suggests that more than one mechanism controls the adsorption process.

### 3.5. Adsorption thermodynamics

Thermodynamic parameters are used for better understanding of the effect of temperature effect on dye adsorption on adsorbents. The parameters involved are; the changes in enthalpy ( $\Delta H$ ), entropy ( $\Delta S$ ), Gibbs free energy ( $\Delta G$ ) and activation energy ( $E_a$ ). Table 8 shows the thermodynamic parameters for the adsorption of RBBR dye onto PPAC. The  $\Delta H$  value obtained is 30.88 in kJ/mol. The positive sign indicates that the process is endothermic in nature. This behavior might be due to the increase of diffusion rate of adsorbate across the external boundary layer and internal pores of adsorbents [8,9].

**Table 7**

Kinetic model constant values for adsorption of RBBR dye onto PPAC at 30 °C.

Model	Kinetic parameters	Initial RBBR dye concentration (mg/L)					
		50	100	200	300	400	500
<b>Pseudo-first-order</b>	$q_e$ exp (mg/g)	29.518	51.714	92.246	131.02	166.87	198.81
	$k_1$ ( $\text{min}^{-1}$ )	0.5831	0.4043	0.4055	0.3968	0.3656	0.3406
	$q_e$ cal (mg/g)	24.964	35.383	78.129	115.89	156.94	194.95
	$R^2$	0.9842	0.9969	0.9908	0.9948	0.7150	0.6326
	$\Delta q_t$ (%)	9.546	7.787	16.682	18.237	19.286	19.80
<b>Pseudo-second-order</b>	$q_e$ cal (mg/g)	34.325	47.049	97.516	152.82	251.47	380.14
	$k_2$ ( $\text{min}^{-1}$ )	0.0313	0.0204	0.0063	0.0030	0.0009	0.0004
	$R^2$	0.9965	0.9986	0.9987	0.9979	0.9989	0.9991
	$\Delta q_t$ (%)	3.256	1.804	1.143	3.328	10.140	18.242
<b>Elovich</b>	$\alpha_{El}$ (mg/g min)	3.913	2.704	0.470	0.267	0.141	0.090
	$\beta_{El}$ ( $\text{g mg}^{-1}$ )	5.3705	7.9482	17.952	26.458	35.765	44.643
	$R^2$	0.9259	0.9882	0.9795	0.9790	0.9813	0.9791
	$\Delta q_t$ (%)	99.369	99.757	99.939	99.971	99.983	99.989
<b>Avrami</b>	$n_{AV}$	0.8191	0.5759	0.8933	0.8023	0.8875	0.9662
	$k_{AV}$ ( $\text{min}^{-1}$ )	0.0097	0.0099	0.0076	0.0059	0.0047	0.0043
	$R^2$	0.9909	0.9891	0.9856	0.9920	0.9649	0.9789

The  $E_a$  value obtained is 17.23 kJ/mol. This value is lower than 40 kJ/mol, indicating that the process follows physisorption mechanism. The adsorption of RBBR dye onto PPAC shows that the rate limiting step in the process is physically controlled [66].  $\Delta S$  value obtained is positive 54.46 J/mol K suggesting that during adsorption at the solid–liquid interface, the degree of freedom increased. Besides, the positive value indicates the randomness at solid–liquid interface reflecting the affinity of adsorbate towards the adsorbent [66,69]. The negative value of  $\Delta G$  indicates that the adsorption process is spontaneous.  $\Delta G$  values obtained are lower than 20 kJ/mol; this further supports the fact that the adsorption process follows physisorption mechanism [9].

### 3.6. Adsorption mechanism

The intraparticle diffusion model was used to study the kinetic mechanism of RBBR dye adsorption. Fig. 8 below showed the plots of intraparticle diffusion model with multi-linear profiles at various initial dye concentrations at 30 °C. From the plots, the first linear sharp region found at the first 150 min might due to the instantaneous adsorption of dye on the external surface of adsorbent or the boundary layer diffusion of solute molecules. In addition, it might due to the strong electrostatic attraction between the dye and adsorbent. The second phase was the gradual adsorption phase, where the intraparticle diffusion is a rate limiting step. The third region was attributed to the final equilibrium stage where the adsorption process starts to slow down due to the high affinity of adsorbate adsorbed on the adsorbent surface. The three different stages having non-zero intercepts suggests that intraparticle diffusion is not the only rate limiting step in the adsorption process. The third phase that does not pass through the origin also confirmed it [69]. The  $k_p$  values for RBBR at all the stages showed an increase as concentration increases. The value of intercept,  $C$  also increased from the first stage to the third stage with increase in initial dye concentration, this might be due to the boundary layer effect (Table 9). The increase in boundary layer thickness would decrease the external mass transfer thus increasing the chance of internal mass transfer [8].

Fig. 9 showed the Boyd plots for adsorption of RBBR dye onto PPAC at 30 °C. The Boyd kinetic mechanism is important in distinguishing the film diffusion from the particle diffusion of adsorbate molecules. The Boyd kinetic mechanism is illustrated by the plot of linearity test of  $B_t$  against time to distinguish between the film diffusion and particle diffusion controlled adsorption. From the figure, the linear lines obtained at all initial concentration of RBBR dye did not pass through the origin. This

**Table 8**  
Thermodynamic parameters for RBBR dye adsorption onto PPAC.

Activated carbon	$\Delta H$ (kJ/mol)	$\Delta S$ (J/mol/K)	$E_a$ (kJ/mol)	$-\Delta G$ (kJ/mol)		
				303 K	318 K	333 K
PPAC	30.88	54.46	17.23	14.25	13.85	12.59

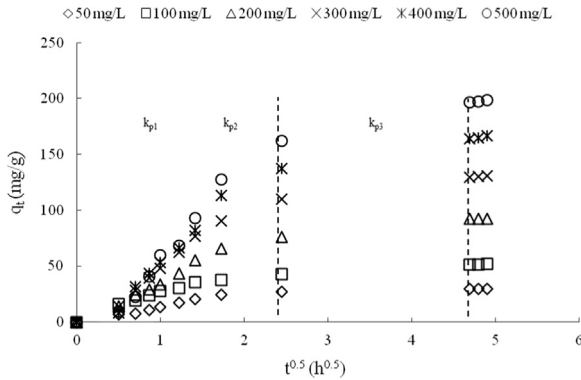


**Fig. 8.** Plots of intraparticle diffusion model for the adsorption of RBBR dye onto PPAC at 30 °C.

**Table 9**  
Intraparticle diffusion model constant for adsorption of RBBR dye onto PPAC at 30 °C.

Dye	Dye initial concentration (mg/L)	50 mg/L	100 mg/L	200 mg/L	300 mg/L	400 mg/L	500 mg/L
RBBR	$K_{p1}$ (mg/gh <sup>1/2</sup> )	13.362	17.245	19.065	28.784	29.876	32.064
	$K_{p2}$ (mg/gh <sup>1/2</sup> )	11.5206	12.8965	31.7052	47.8827	63.2839	80.8634
	$K_{p3}$ (mg/gh <sup>1/2</sup> )	0.0382	0.0479	2.0852	6.1488	12.3299	14.6961
	$C_1$	0.1564	0.1768	0.1876	0.1965	0.1978	0.1983
	$C_2$	0.8618	1.9773	4.3363	9.6105	13.7688	26.4413
	$C_3$	29.2831	41.4475	92.0577	100.8227	106.2672	146.2175
	$(R_1)^2$	1	1	1	1	1	1
	$(R_2)^2$	0.9030	0.9080	0.9422	0.9534	0.9718	0.9698
	$(R_3)^2$	0.9999	0.8609s	0.9196	0.9632	0.9303	0.9187

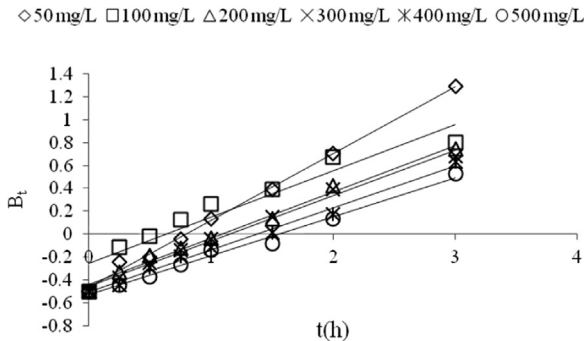


**Fig. 9.** Boyd plots for adsorption of RBBR dye onto PPAC at 30 °C.

behavior is due to the differences in the rate of mass transfer in the first and second stages by external mass transfer or film diffusion, where the particle diffusion was the limiting step. If the linear plot passes through the origin, we can say that the adsorption process is governed by particle diffusion mechanism, however, in this case, it does not pass through the origin, it therefore shows that the adsorption is governed by film diffusion.

#### 4. Conclusion

PPAC was successfully prepared using microwave assisted and KOH activation techniques for the adsorption of RBBR dye. BET surface area and total pore volume for PPAC of 941.02 m<sup>2</sup>/g and 0.47 cm<sup>3</sup>/g, makes the adsorbent comparable with the commercial F300 and F400 AC from Merck. A high value of  $Q_m$  revealed that the adsorbent prepared is very effective compared to other ones studied in literature having high adsorption capacity as well as fast uptake of RBBR dye in aqueous solutions. The improvement in surface and textural properties was attributed to the technique and reagents used for modification. Thermodynamic studies indicated that the adsorption process is endothermic and spontaneous. The adsorption characteristics of the modified PPAC presented in this paper make this adsorbent a promising one in the field of adsorption for the removal of synthetic dye in wastewater treatment.

#### Acknowledgments

The financial support in form of grants from USM, the three months USM-TWAS Visiting Researcher Fellowship, FR number: 3240268492 awarded to the corresponding author and the accumulated leave granted to Dr. O. S. Bello by his home institution to utilize the fellowship is thankfully recognized.

#### References

- [1] G. McKay, G.A. Sweeney, Principles of dye removal from textile effluents, *Water Air Soil Pollut.* 4 (1980) 3–11.
- [2] D. Peterson, *Colorants and Auxiliaries: Organic Chemistry and Application Properties*, in: J. Shore (Ed.), *BTTC- Shirley*, Manchester 1990, pp. 32–72.
- [3] L.C. Morais, O.M. Freitas, E.P. Goncalves, L.T. Vasconcelos, G.C.G. Beca, Reactive dyes removal from wastewater by adsorption on eucalyptus bark: variable that define the process, *Water Res.* 33 (1999) 979–998.
- [4] T. Robinson, G. Mc Mullan, R. Marchant, P. Nigam, Remediation of dyes in textile effluent, a critical review on current treatment technologies with a proposed alternative, *Bioresour. Technol.* 77 (2001) 247–255.
- [5] D. Ahn, W. Chang, T. Yoon, Dyestuff waste water treatment using chemical oxidation, physical adsorption and fixed bed biofilm process, *Process Biochem.* 34 (1999) 429–439.
- [6] T. Deveci, A. Unyayar, M.A. Mazmanci, Production of remazol brilliant blue r decolorising oxygenase from the culture filtrate of *Funalia trogii* ATCC200800, *J. Mol. Catal. B Enzymatic* 30 (2004) 25–32.
- [7] I. Eichlerová, L. Homolka, O. Benada, O.K.T. Hubálek, F. Nerud, Decolorization of orange g and remazol brilliant blue r by the white rot fungus *Dichomitus squalens*: toxicological evaluation and morphological study, *Chemosphere* 69 (2007) 795–802.
- [8] O.S. Bello, M.A. Ahmad, N. Ahmad, Adsorptive features of banana (*Musa paradisiaca*) stalk-based activated carbon for malachite green dye removal, *Chem. Ecol.* 28 (2012) 153–167.
- [9] O.S. Bello, T.A. Fatona, F.S. Falaye, O.M. Osuolale, V.O. Njoku, Adsorption of eosin dye from aqueous solution using groundnut hull-based activated carbon: kinetic, equilibrium, and thermodynamic studies, *Environ. Eng. Sci.* 29 (2012) 186–194.
- [10] O.S. Bello, Adsorptive removal of malachite green with activated carbon prepared from oil palm fruit fibre by KOH activation and CO<sub>2</sub> gasification, *S. Afr. J. Chem.* 66 (2013) 32–41.
- [11] O.S. Bello, M.A. Ahmad, Adsorptive removal of a synthetic textile dye using coca pod husks, *Toxicol. Environ. Chem.* 93 (2011) 1298–1308.
- [12] O.S. Bello, M.A. Ahmad, Adsorption of dyes from aqueous solution using chemical activated mango peels. In: *Proceedings of the 2nd International Conference on Environmental Science and Technology (ICEST)*, 2, 2011, pp. 108–113.
- [13] N.E.M. Yahaya, M.F. Pakir, M. Latiff, I. Abustan, I.O.S. Bello, M.A. Ahmad, Process optimization for Zn(II) removal by activated carbon prepared from rice husk using chemical activation, *Int. J. Eng. Technol.* 10 (2010) 132–136.
- [14] N.E.M. Yahaya, M.F. Pakir, M. Latiff, I. Abustan, I.O.S. Bello, M.A. Ahmad, Effect of preparation conditions of activated carbon prepared from rice husk by CO<sub>2</sub> activation for removal of Cu(II) from aqueous solution, *Int. J. Eng. Technol.* 10 (2010) 47–51.
- [15] N.E.M. Yahaya, M.F. Pakir, M. Latiff, I. Abustan, I.O.S. Bello, M.A. Ahmad, Adsorptive removal of Cu(II) using activated carbon prepared from rice husk by ZnCl<sub>2</sub> activation and subsequent gasification with CO<sub>2</sub>, *Int. J. Eng. Technol.* 11 (2011) 207–211.
- [16] N.E.M. Yahaya, M.F. Pakir, M. Latiff, I. Abustan, I.O.S. Bello, M.A. Ahmad, Fixed bed column study for Cu(II) removal from aqueous solutions using rice husk based activated carbon, *Int. J. Eng. Technol.* 11 (2011) 248–252.



- [17] O.S. Bello, I.A. Adeogun, J.C. Ajaelu, J.C.E.O. Fehintola, Adsorption of methylene blue onto activated carbon derived from periwinkle shells: kinetics and equilibrium studies, *Chem. Ecol.* 24 (2008) 285–295.
- [18] O.S. Bello, M.A. Ahmad, Coconut (*Cocos nucifera*) shell based activated carbon for the removal of malachite green dye from aqueous solutions, *Sep. Sci. Technol.* 47 (2012) 903–912.
- [19] O.S. Bello, B. Semire, Equilibrium, kinetic and quantum chemical studies on the adsorption of Congo red using *Imperata cylindrica* leaf powder activated carbon, *Toxicol. Environ. Chem.* 94 (2012) 1114–1124.
- [20] O.S. Bello, M.A. Ahmad, Preparation and characterization of activated carbon derived from rubber seed coat, *Chemistry: Bulg. J. Sci. Edu.* 21 (2012) 389–395.
- [21] O.S. Bello, O.A. Oluwole, V.O. Njoku, Fly ash: an alternative to powdered activated carbon for the removal of eosin dye from aqueous solutions, *Bull. Chem. Soc. Ethiopia* 27 (2013) 191–204.
- [22] H. Altaher, T.E. Khalil, R. Abubeah., The effect of dye chemical structure on adsorption on activated carbon: a comparative study, *Color. Technol.* 130 (2014) 205–214.
- [23] A.M. Aljeboree, A.N. Alshirifi, A.F. Alkaim. Kinetics and equilibrium study for the adsorption of textile dyes on coconut shell activated carbon. *Arab. J. Chem.* (2014). <http://dx.doi.org/10.1016/j.arabjc.2014.01.020>.
- [24] L. Yu, Y. Luo., The adsorption mechanism of anionic and cationic dyes by Jerusalem artichoke stalk-based mesoporous activated carbon, *J. Environ. Chem. Eng.* 2 (2014) 220–229.
- [25] V.M. Vučurović, R.N. Razmovski, U.D. Miljić, V.S. Puškaš, Removal of cationic and anionic azo dyes from aqueous solutions by adsorption on maize stem tissue, *J. Taiwan Inst. Chem. Eng.* 45 (2014) 1700–1708.
- [26] A. Pirkarami, M.E. Olya, Removal of dye from industrial wastewater with an emphasis on improving economic efficiency and degradation mechanism, *J. Saudi. Chem. Soc.* (2013). <http://dx.doi.org/10.1016/j.jscs.2013.12.008>.
- [27] A. Akyol, Treatment of paint manufacturing wastewater by electrocoagulation, *Desalination* 285 (2012) 91–99.
- [28] K.Y. Foo, B.H. Hameed, Textural porosity, surface chemistry and adsorptive properties of durian shell derived activated carbon prepared by microwave assisted NaOH Activation, *Chem. Eng. J.* 187 (2012) 53–62.
- [29] I. Langmuir, The adsorption of gases on plane surfaces of glass, mica and platinum, *J. Am. Chem. Soc.* 40 (1918) 1361–1403.
- [30] H.M.F. Freundlich, Over the adsorption in solution, *J. Phys. Chem.* 57 (1906) 385–471.
- [31] M.I. Temkin, V. Pyzhev, Kinetics of ammonia synthesis on promoted iron catalyst, *Acta Physiochim. USSR* 12 (1940) 327–356.
- [32] M.M. Dubinin, L.V. Radushkevich, Equation of the characteristic curve of activated charcoal, *Proc. Acad. Sci.: Phys. Chem. Sect. USSR* 55 (1947) 331–333.
- [33] R. Sips, Combined form of Langmuir and Freundlich equations, *J. Chem. Phys.* 16 (1948) 490–495.
- [34] W.R. Vieth, K.J. Sladek, A model for diffusion in a glassy polymer, *J. Coll. Sci.* 20 (1965) 1014–1033.
- [35] F. Brouers, O. Sotolongo, F. Marquez, J.P. Pirard, Microporous and heterogeneous surface adsorption isotherms, *Phys. A: Stat. Mech. Appl.* 349 (2005) 271–282.
- [36] C.J. Radke, J.M. Prausnitz, Adsorption of organic solutes from dilute aqueous solution on activated carbon, *Ind. Eng. Chem. Fund.* 11 (1972) 445–451.
- [37] S. Lagergren, Zur Theorie der Sogenannten, Adsorption Geloester Stoffe, *Veternskapsakad, Handlingar*, 24, 1898 pp. 1–39..
- [38] Y.S. Ho, G. McKay, Pseudo-second order model for sorption processes, *Proc. Biochem.* 34 (1999) 451–465.
- [39] C. Aharoni, M. Ungarish, Kinetics of activated chemisorptions. Part I: the non-Elovichian part of the isotherm, *J. Chem. Soc. Farad. Trans.* 72 (1976) 265–268.
- [40] M. Avrami, Kinetics of phase change: transformation-time relations for random distribution of nuclei, *J. Chem. Phys.* 8 (1940) 212–224.
- [41] W.J. Weber, J.C. Morris, Kinetics of adsorption on carbon from solution, *J. Sanit. Eng. Div.* 89 (1962) 31–59. (ASCE).
- [42] F.C. Wu, R.I. Tseng, R.S. Jung, Kinetic modeling of liquid-phase adsorption of reactive dyes and metal ions on chitosan, *Water Res.* 35 (2001) 613–618.
- [43] S. Wang, Y. Boyjoo, A. Choueib, Z.H. Zhu, Removal of dyes from aqueous solution using fly ash and red mud, *Water Res.* 39 (2005) 129–138.
- [44] IUPAC, IUPAC manual of symbols and terminology, *Pure Appl. Chem* 31 (1972) 579–638.
- [45] O.S. Bello, T.S. Tan, M.A. Ahmad, Adsorption of remazol brilliant violet-5R reactive dye from aqueous solution by cocoa pod husk-based activated carbon: kinetic, equilibrium and thermodynamic studies, *Asia-Pacif. J. Chem. Eng.* 7 (2012) 378–388.
- [46] M.A. Ahmad, R. Alrozi, Optimization of preparation conditions for mangosteen peel-based activated carbons for the removal of remazol brilliant blue R using response surface methodology, *J. Chem. Eng.* (2010) 883–890.
- [47] H. Chen, Z. Hashisho, Effects of microwave activation conditions on the properties of activated oil sands coke, *Fuel Proc. Technol.* 102 (2012) 102–109.
- [48] A. Faisal, W.M.A. Wan Daud, M.A. Ahmad, R. Radzi, The effects of acid leaching on porosity and surface functional groups of cocoa (*Theobroma cacao*)-shell based activated carbon, *Chem. Eng. Res. Design* 90 (2013) 1–11.
- [49] I. Nazri, Z.A. Ahmad, M.A. Ahmad, N. Ahmad, S.K. Sulaiman, Optimization of process variables for malachite green dye removal using rubber seed coat based activated carbon, *Int. J. Eng. Technol.* 11 (2011) 305–311.
- [50] Y. Sun, P.A. Webley, Preparation of activated carbons from corn cob with large specific surface area by a variety of chemical activators and their application in gas storage, *Chem. Eng. J.* 162 (2010) 883–892.
- [51] M. Auta, B.H. Hameed, Optimized waste tea activated carbon for adsorption of methylene blue and acid blue 29 dyes using response surface methodology, *Chem. Eng. J.* 175 (2011) 233–243.
- [52] D.K. Mahmoud, M.A. Salleh, W.A. Wan, Abdul Karim, A. Idris, A. Z. Zainal Abidin, Batch adsorption of basic dye using acid treated kenaf fiber char: Equilibrium, kinetic and thermodynamic studies, *Chem. Eng. J.* 181–182 (2012) 449–457.
- [53] K. Li, Z. Zheng, X. Huang, G. Zhao, J. Feng, J. Zhang, Equilibrium, kinetic and thermodynamic studies on the adsorption of 2-nitroaniline onto activated carbon prepared from cotton stalk fibre, *J. Hazard. Mater.* 166 (2009) 213–220.
- [54] A. Bhatnagar, A.K. Minocha, Conventional and non-conventional adsorbents for removal of pollutants from water, *Indian J. Chem. Technol.* 13 (2006) 203–217.
- [55] N.M. Mahmoodi, B. Hayati, M. Arami, C. Lan, Adsorption of textile dyes on pine cone from colored wastewater: kinetic, equilibrium and thermodynamic studies, *Desalination* 268 (2011) 117–125.

- [56] P. Nowicki, H. Wachowska, R. Pietrzak, Active, carbons prepared by chemical activation of plum stones and their application in removal of NO<sub>2</sub>, *J. Hazard. Mater.* 181 (2010) 1088–1094.
- [57] H.P. Boehm, Surface, Oxides on carbon and their analysis: a critical assessment, *Carbon* 40 (2002) 145–149.
- [58] P. Sathishkumar, M. Arulkumar, T. Palvannan, Utilization of agro-industrial waste *Jatropha curcas* pods as an activated carbon for the adsorption of reactive dye remazol brilliant blue R (RBBR), *J. Cleaner Prod.* 22 (2012) 67–75.
- [59] F. Helfferich, Ion-Exchange, McGraw-Hill, New York, 1962.
- [60] O.S. Bello, M.A. Ahmad, Response surface modelling and optimization of remazol brilliant blue reactive dye removal using periwinkle shell based activated carbon, *Sep. Sci. Technol.* 46 (2011) 2367–2379.
- [61] D. Mahanta, G. Madras, S. Radhakrishnan, S. Patil, Adsorption and desorption kinetics of anionic dyes on doped polyaniline, *J. Phys. Chem. B* 113 (2009) 2293–2299.
- [62] V. Janaki, B.T. Oh, K. Shanthi, K.J. Lee, A.K. Ramasamy, S. Kamala-Kannan., Polyaniline/chitosan composite: an eco-friendly polymer for enhanced removal of dyes from aqueous solution, *Synth. Met.* 162 (2012) 974–980.
- [63] V. Janaki, K. Vijayaraghavan, A. Ramasamy, K. Lee, B. Oh, S.K. Kannan, S.K., Competitive adsorption of reactive orange 16 and reactive brilliant blue r on polyaniline/bacterial extracellular polysaccharides composite—a novel eco-friendly polymer, *J. Hazard. Mater.* 242 (2012) 110–117.
- [64] S. Kara, C. Aydinler, E. Demirbas, M. Kobya, N. Dizge, Modeling the effects of adsorbent dose and particle size on the adsorption of reactive textile dyes by fly ash, *Desalination* 212 (2007) 282–293.
- [65] A. Ergene, K. Ada, S. Tan, H. Katircioğlu, Removal of remazol brilliant blue R dye from aqueous solutions by adsorption onto immobilized *Scenedesmus quadricauda*: equilibrium and kinetic Modeling studies, *Desalination* 249 (2009) 1308–1314.
- [66] B. Mi-Hwa, B.C.O. Ijagbemi, O. Se-Jin, D.S. Kim, Removal of malachite green from aqueous solution using degreased coffee bean, *J. Hazard. Mater.* 176 (2010) 820–828.
- [67] K.H. Chu, Removal of copper from aqueous solution by chitosan in prawn shell: adsorption equilibrium and kinetics, *J. Hazard. Mater.* 90 (2002) 77–95.
- [68] C. Theivarasu, S. Mylsamy, Removal of malachite green from aqueous solution by activated carbon developed from cocoa (*Theobroma Cacao*) shell - A kinetic and equilibrium studies, *E–J. Chem.* 8 (2011) 363–371.
- [69] Y. Onala, C. Akmil-Başara, E. Didem, C.S Özdemira, D. Tolga, Adsorption kinetics of malachite green onto activated carbon prepared from Tunçbilek Lignite, *J. Hazard. Mater.* 128 (2006) 150–157.